Design of the compliant gripper and pipe flow control

ME-763 mini project

Instructor: Prof. Bishakh Bhattacharya

Mentor: Suraj Mishra

Abhishek Kumar(220043)

Avinash Bhashkar(241050632)

Raj Kumar(241050620)

IIT Kanpur

Contents

Literature survey

Author(s) & Year	Synthesis Method	Specifications	Intended Application
Goh et al., 2022	**3D printing**		**Soft robotic grippers**
Alizadehyazdi et al., 2018	Etching of copper layer on Kapton sheet	9 µm thick copper layer, 13-micron Kapton sheet	**Electrode pattern for actuation**
Wang et al., 2022	**3D printing of polyethylene (PE)**	Anisotropic PE layer with filaments printed at a determined angle	**Helical deformation in a single structure**
Li et al., 2019	Self-folding of laminate structure, 3D printing of molds for silicone rubber skeleton, TPU-coated nylon sheet, Latex rubber balloon skin	Self-folded skeleton gripper achieved 30 N holding force, rubber skeleton gripper achieved 120 N	**Gripping**
Various (review), 2022	**Fused Filament Fabrication (FFF)**	Uses thermoplastics like PLA, Nylon, TPU	**Soft gripper fabrication**
Various (review), 2022	**Selective Laser Sintering (SLS)**	Powder bed, porosity 4-10%	**Pneumatic soft grippers, vacuum grippers**
Mousavi et al., 2022	FFF with conductive filament and carbon nanotube fillers	Gauge factor of 1342	**Multidirectional tactile sensor**
Moore and Williams, 2022	Material jetting of elastomers	Fatigue life of 10^6 cycles at 20% elongation, 1.7 Hz test frequency	**Soft actuators**
Shintake et al., 2018			**Soft robotic grippers**
Simone et al., 2018	3D printed tendon-driven structures	Three independently actuated fingers	**Prosthetic gripper**
Lan et al., 2018	SMA wires, poly-oxymethylene flexible frame	Two 10 mm fingers, self-sensing	**Microgripper manipulation**
Odhner et al., 2014	Underactuated fingers with compliant mechanics	Fingertip grasps, in-hand grasp transitions, and basic tool use	**Mobile robots**
Magdy et al., 2023	Double-inverted 2D pantograph with a guiding mechanism	Micro displacement, miniaturizing ratio 0.5, micro displacement 100µm, grasping objects 100µm to 1500µm	**Micro-manipulation**
Wang et al., 2017	Integrating soft composite actuator with stiffness changeable material	Each finger has two hinges with 55-fold stiffness change.	**Adaptive grasping**
Then Mozhi et al., 2023	SMA wires	Displacement amplification gain of 3.7, maximum tip displacement up to 1.2 cm, object handling up to 0.012m and 35g	**Monolithic compliant gripper**

Cad model and geometry

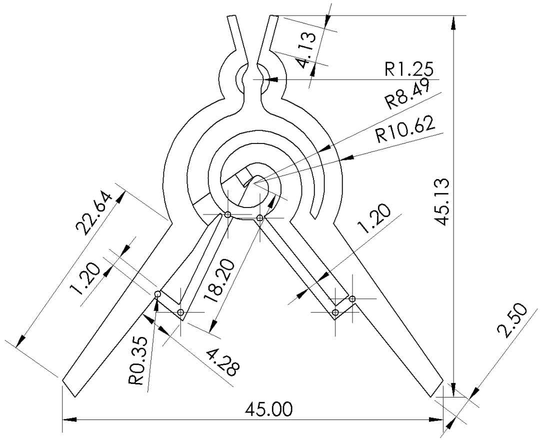

Fig 1(a). Rigid body cad model

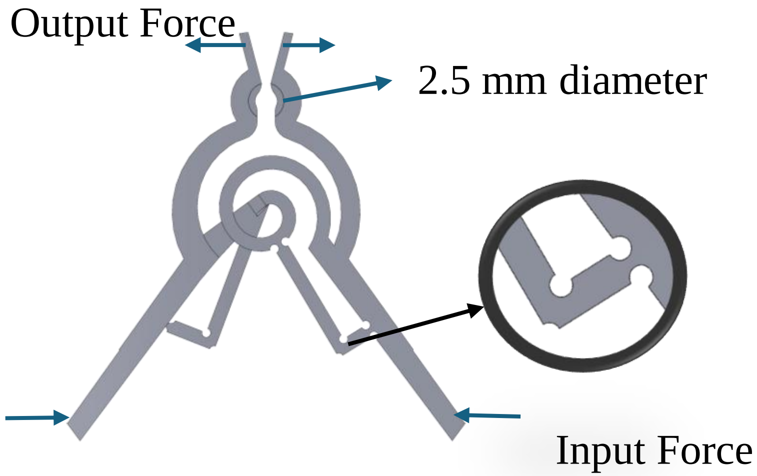

1(b). Pseudo rigid body model cad

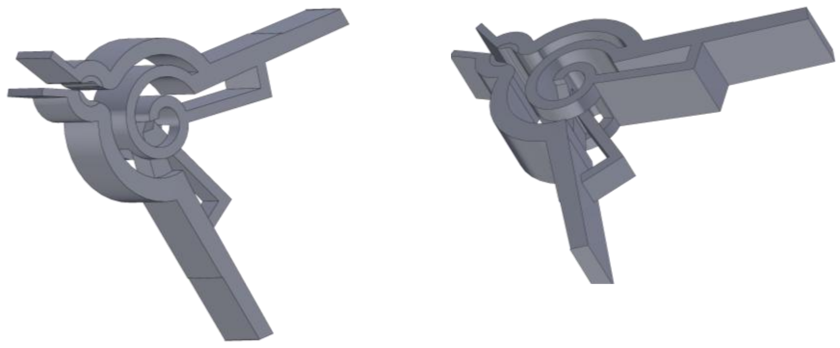

Fig 1(c). Isometric view of the CAD model

- Weight -3 gm
- Material PLA+
- Dimensions 46x46x11 mm

- Novelty:
  - Spiral spring as compliant and energy storing element.
  - Life cycle is higher than other designs
  - It is simple and useful for intravenous drug infusion
  - There is no study on such model in compliant mechanisms literature as per our understanding.

Fig2 Animation of CAD model's functionality

Kinematics and force-deflection analysis

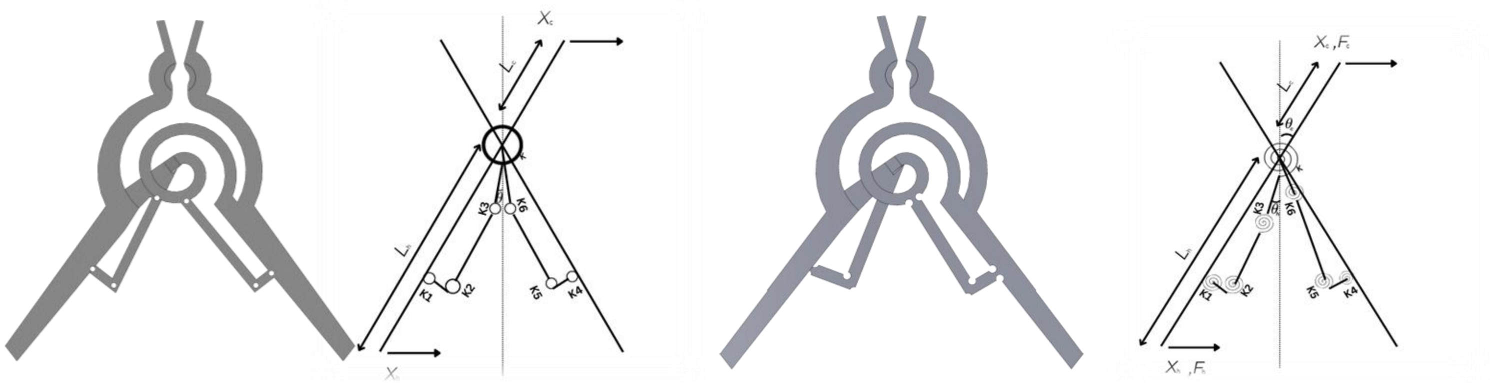

Fig 3(a). Rigid body cad model(Kinematic representation)   (b). Pseudo rigid body model

Where:

- F_h: Input force
- F_c: Output force
- X_h: Input displacement
- X_c: Output displacement

$$X_h = X_c \cdot \frac{L_h}{L_c} \cdot \frac{\sin(\theta_h)}{\sin(\theta_c)}$$

$$F_h = F_c \cdot \frac{L_c}{L_h} \cdot \frac{\sin(\theta_c)}{\sin(\theta_h)}$$

$$F_c \cdot X_c = F_h \cdot X_h$$

Kino-static analysis

Moment Balance at Pivot:

$$M = \sum \tau = \tau_s + (F_{in} L_h) - (F_{out} L_c) = 0$$

$$-k\theta_h - k_1\theta_1 - k_2\theta_2 - k_3\theta_3 + k_4\theta_4 + k_5\theta_5 + k_6\theta_6 + F_{in}L_h - F_{out}L_c = 0$$

Solving for F_{out}:

$$F_{out} = \frac{k\theta_h + k_1\theta_1 + k_2\theta_2 + k_3\theta_3 - k_4\theta_4 - k_5\theta_5 - k_6\theta_6 + F_{in}L_h}{L_c}$$

where $\theta_h, \theta_1, \theta_2, \theta_3, \theta_4, \theta_5, \theta_6$ are variables.

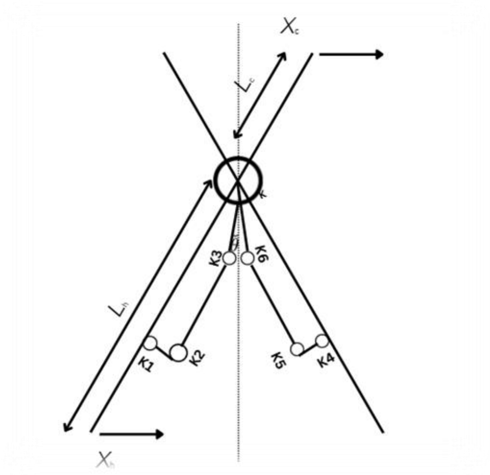

Fig 4(a). Kinematic representation

Force-Deflection Relationship and Pseudo Virtual Work Application

Force-Deflection Relationship Here, Let the spring constant of the torsional spring be K_0, So

$$F_1 L_1 = K_0 \theta$$

$$\theta = \frac{F_1 L_1}{K_0}$$

Now let the other end displaced by x_2, So,

$$x_2 = L_2 \times \theta = \frac{F_1 L_1 L_2}{K_0}$$

$$x_2 = \frac{F_1 L_1 L_2}{K_0}$$

So, Required force to deflect the other end by x,

$$F_1 = F_{req} = \frac{K_0 x_2}{L_1 L_2}$$

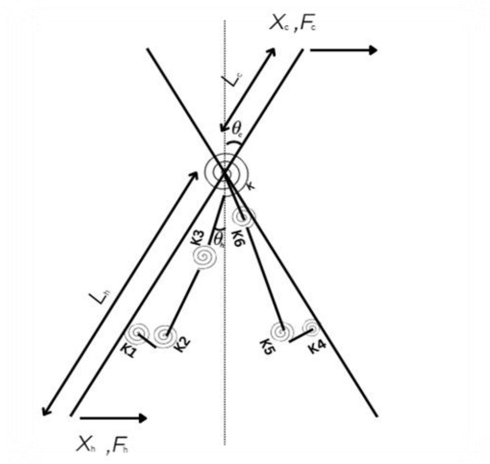

4(b). Pseudo rigid body model

Results

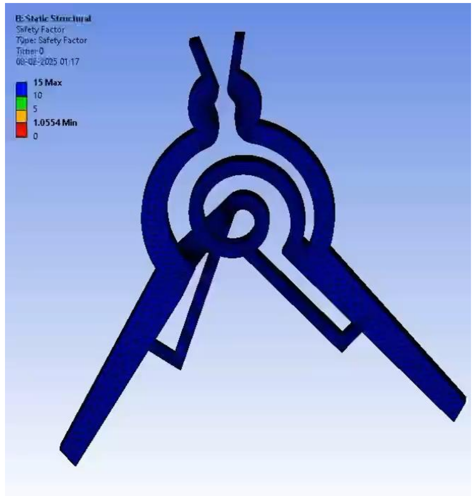

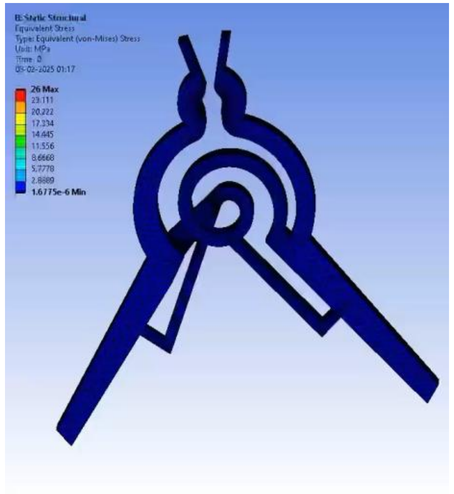

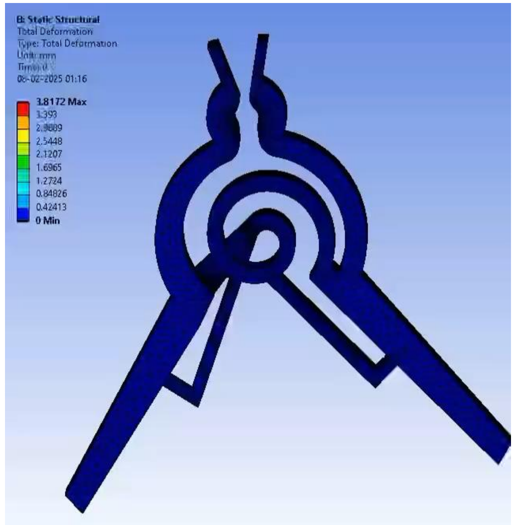

- **Design Efficiency:** The 3D-printed PLA+ microgripper (46×46×11 mm46×46×11 mm, 3 gm)
achieves a miniaturizing ratio of 0.5 and handles objects up to 4mm, making it suitable for medical applications requiring compact, applications.

- **Force-Displacement:** Kinematic equations and pseudo-rigid body modeling ensure a balance between input force and output displacement,
critical for precise flow control in drug delivery systems.

- **Material and Structural Performance:** FEA validates the design’s robustness, with deformation limited to 3.3563 mm3.3563 mm under stress, confirming PLA+’s suitability for high-cycle fatigue applications.

- **Stress-Strain Optimization via Young's Modulus:** The PLA+ material's Young's modulus (~2.06–3.64 Gpa) enables controlled stress distribution under operational loads.

- **Comparative Advantage:** The design outperforms existing methods (e.g., SMA wires,) by integrating stiffness-changeable materials and
achieving a 55-fold stiffness variation per hinge, enhancing adaptive grasping capabilities1.

FEA Analysis

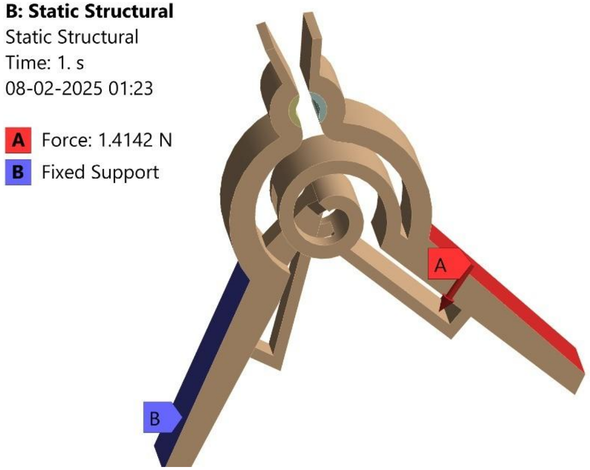

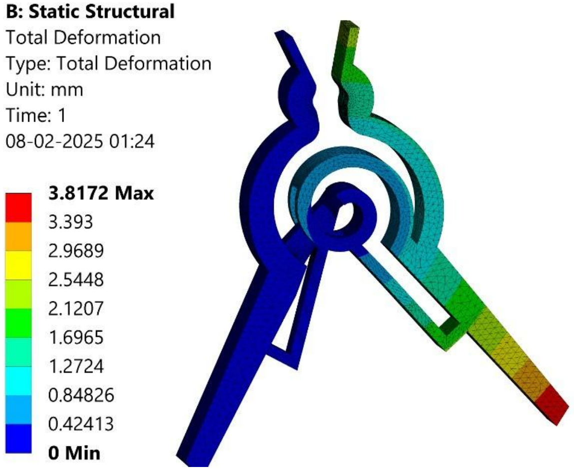

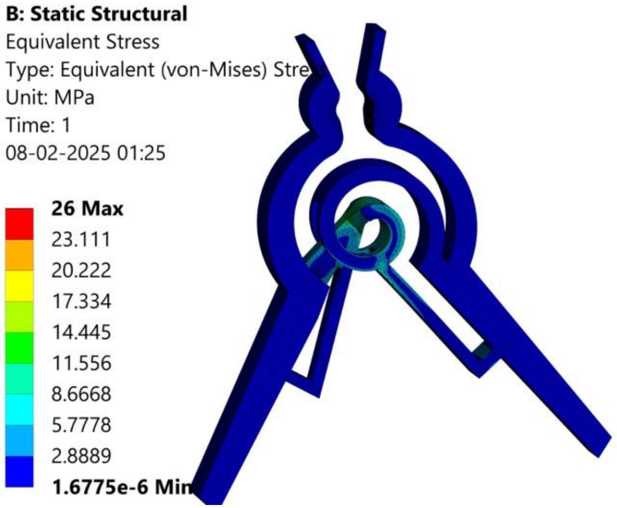

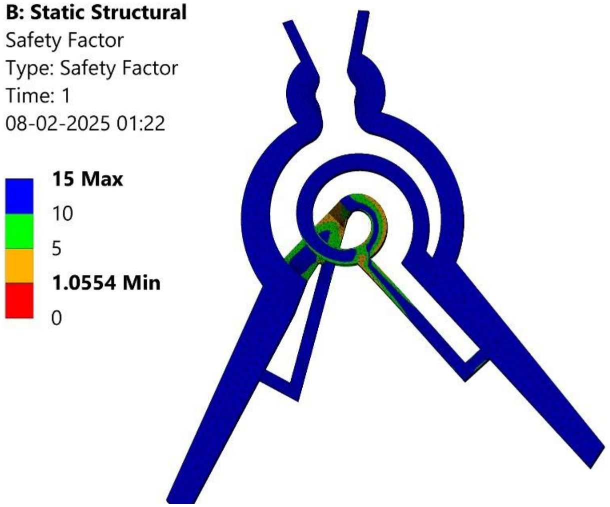

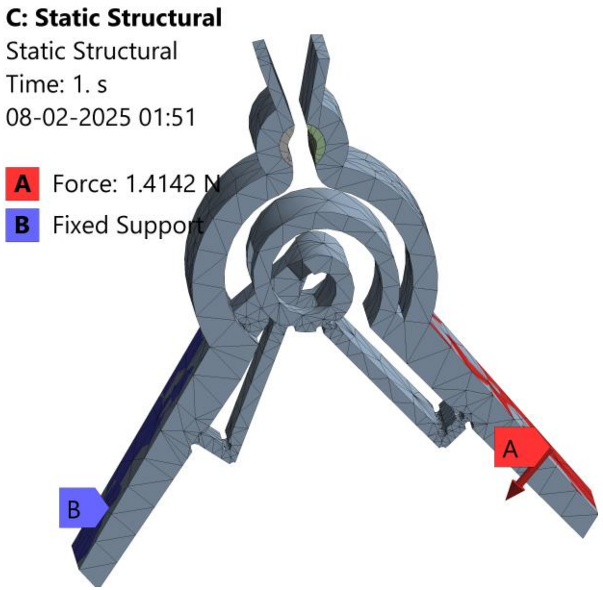

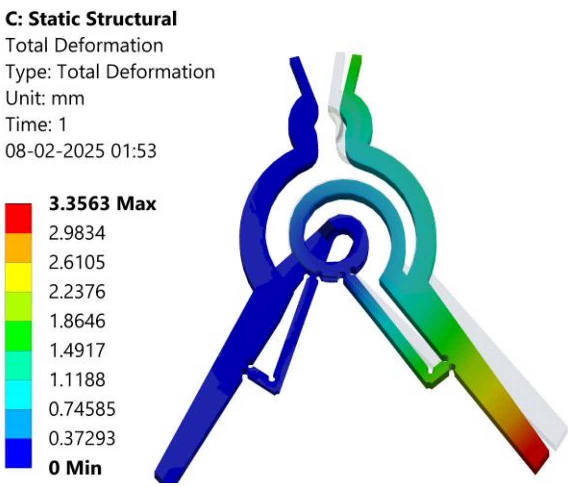

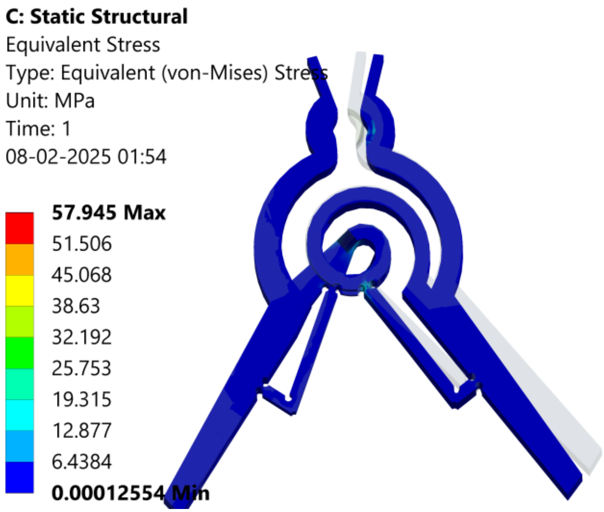

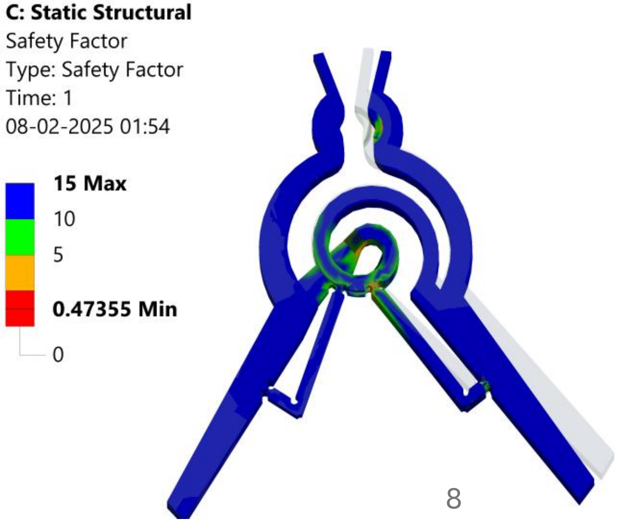

Force Deflection results

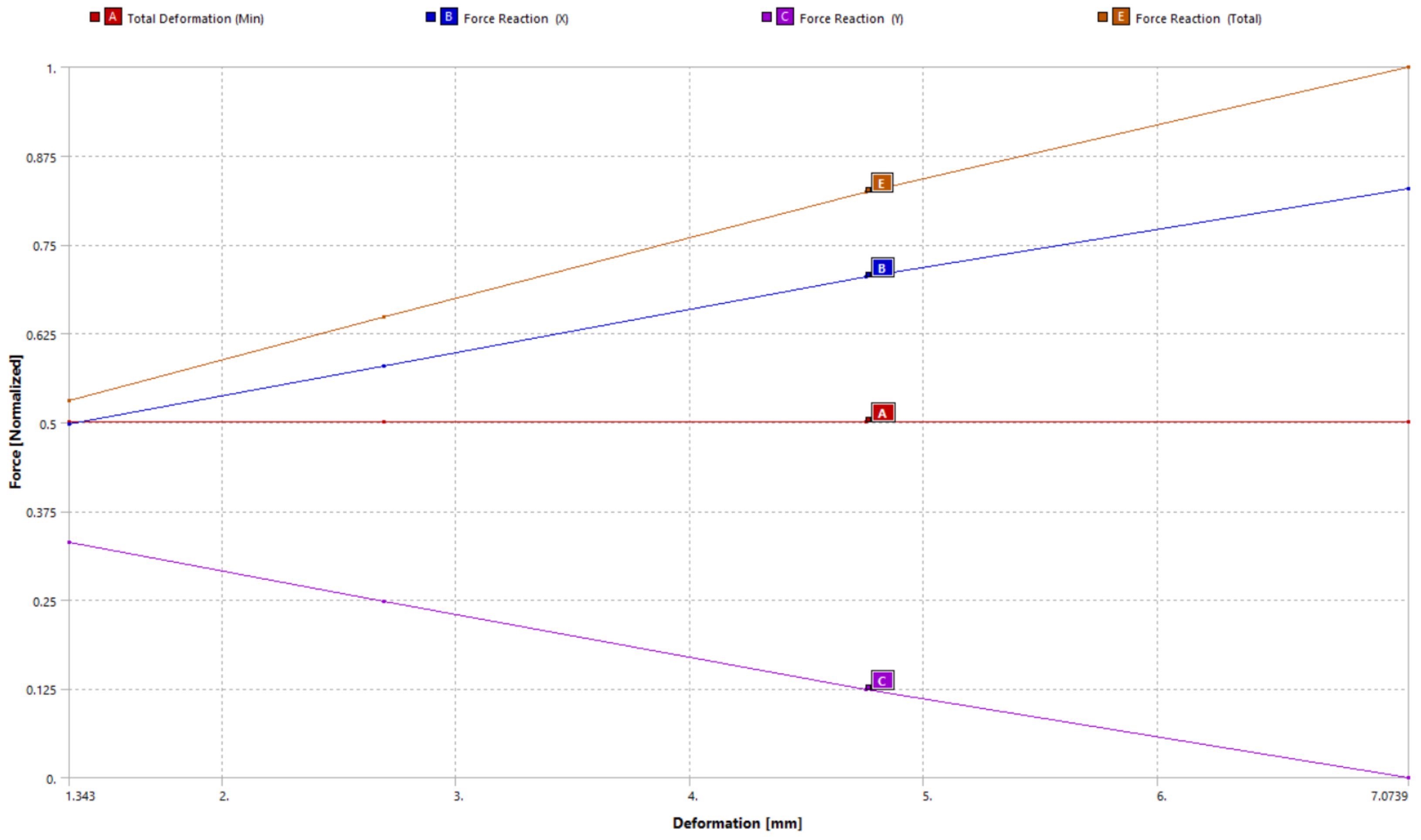

Figure 6. Total deformation vs Force plot form FEM solver

- **Force Reaction in X and Y:** The blue line (B) (Force Reaction in X) shows an increasing trend with deformation.
  The purple line (C) (Force Reaction in Y) decreases as deformation increases.
  - Total Force Reaction:The brown line (E) represents the total force reaction, showing a linear increase with deformation.
  - Deformation Range: The x-axis spans from approximately 1.34 mm to 7.07 mm.
  - Normalization Used: Forces are presented in a normalized form for easier comparison.

Force Deflection results

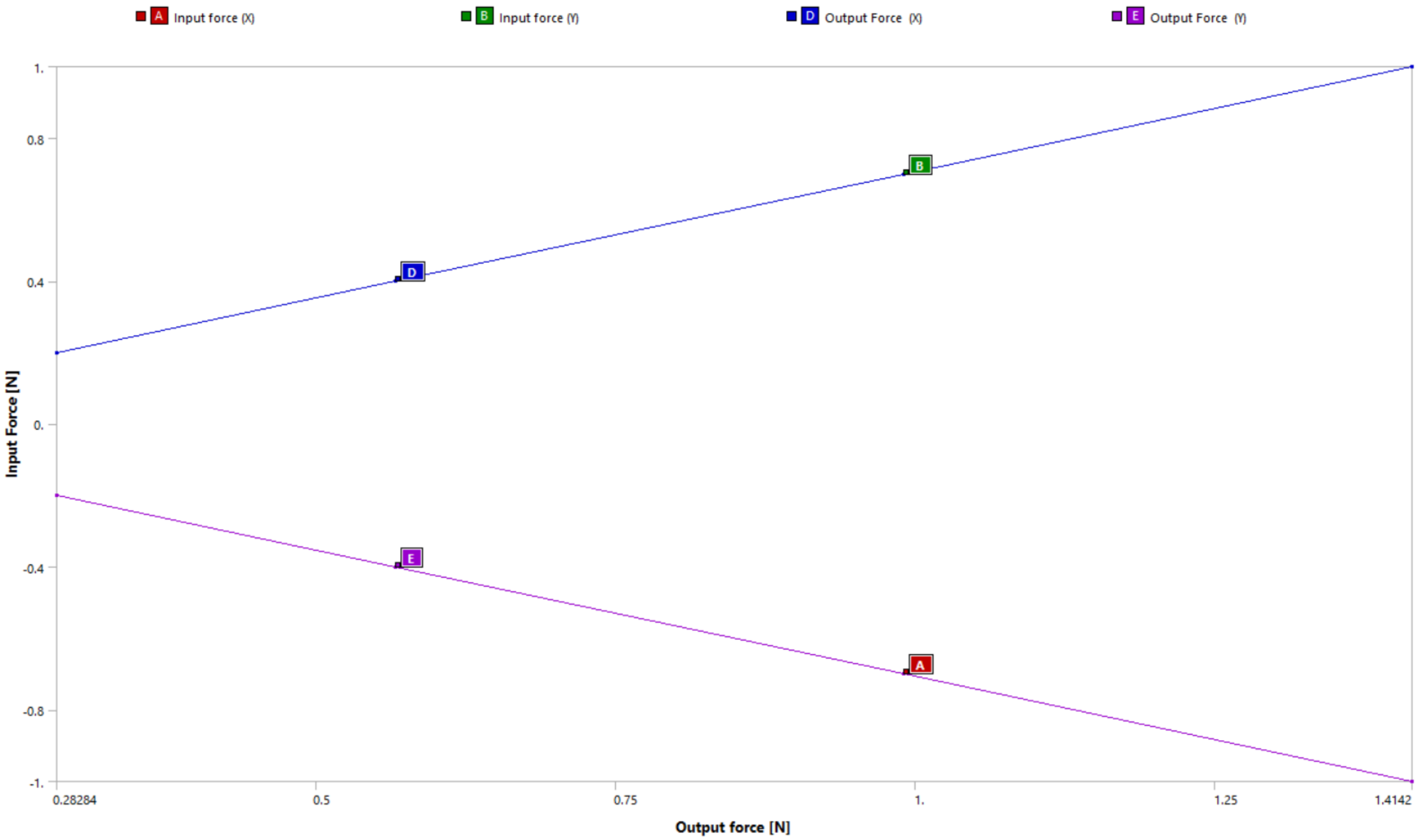

Figure 7. Input force vs Output force plot form FEM solver

Key Observations:

- **Linear Relationships:** The plot indicates a nearly linear correlation between input and output forces, suggesting a proportional system behavior.
- The opposing nature of force reactions in different directions suggests the presence of constraints or reactive forces in the system.
- The symmetry in force distribution may indicate a balanced mechanical structure.

Fatigue analysis

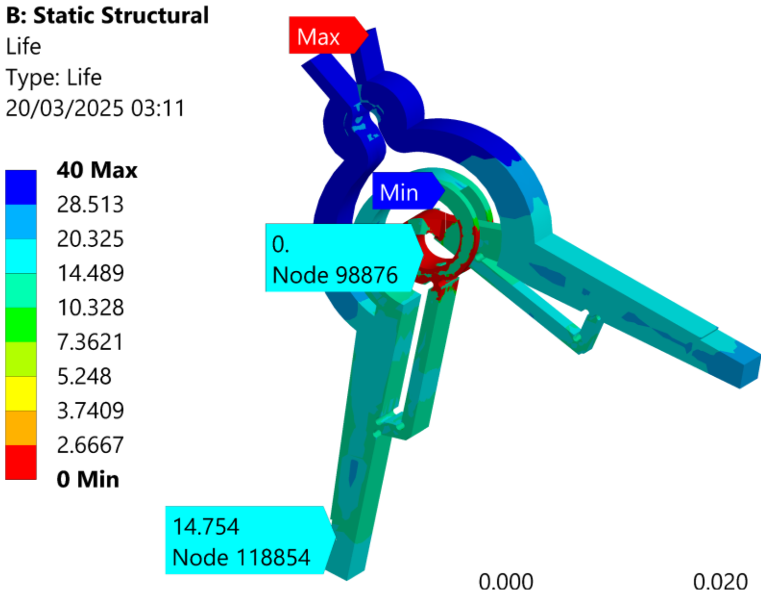

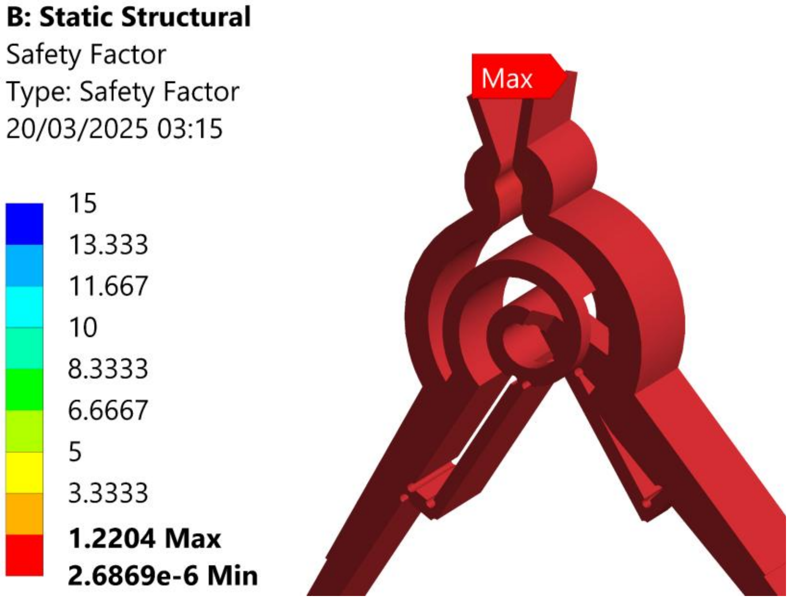

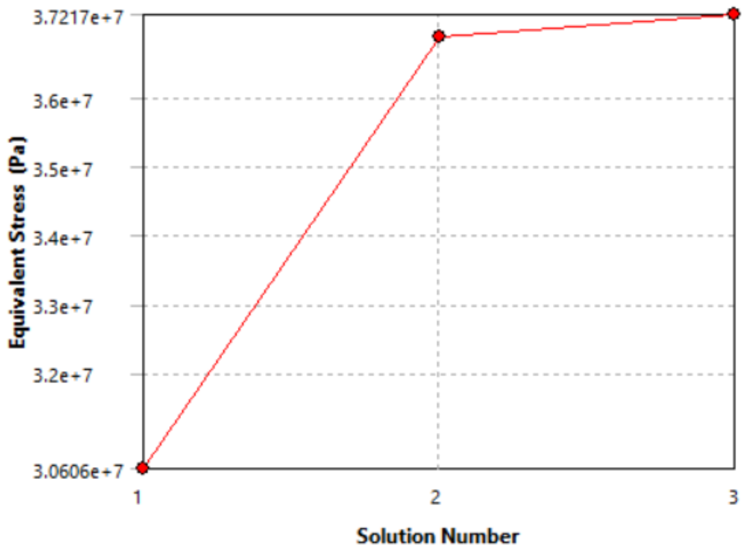

	Equivalent Stress (Pa)	Change (%)	Nodes	Elements
1	3.0606e+007		10360	5014
2	3.6884e+007	18.605	28989	16556
3	3.7217e+007	0.90034	112745	72666

Figure 5. Convergence

- Blue regions indicate higher fatigue life
    - Red regions indicate lower fatigue life
- **Min and Max Life Values:**
    - Minimum life (Node 98876) = 0 cycles
    - Maximum life = 40 cycles
- **Observation:**The red region at the joint connection suggests a high-stress concentration area, possibly due to cyclic loading.

Min and Max Safety Factor Values:

- Minimum safety factor = 2.6869e-6
- Maximum safety factor = 1.2204

- **Observation:** The critical failure zones overlap with the low-fatigue life regions, confirming potential failure at joint connections.

The solution converges after the third iteration, meaning the **FEM model has stabilized** and further refinements wouldn't change results significantly.

Controller for pipe flow control

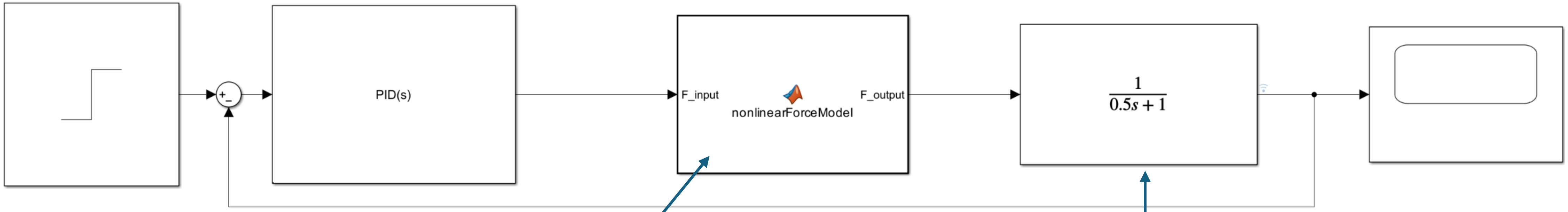

Required force to deflect the other end by x,

$$F_1 = F_{req} = \frac{K_0 x_2}{L_1 L_2}$$

$$P(s) = \frac{K_p}{\tau_p s + 1}$$

Where,

$$K_p = \frac{F_{out}}{F_{in}} = \frac{K_0 + k_1 \ldots}{L_c + (\frac{L_c}{L_h})}$$

$$\tau_p = 0.5$$

Controller for pipe flow control

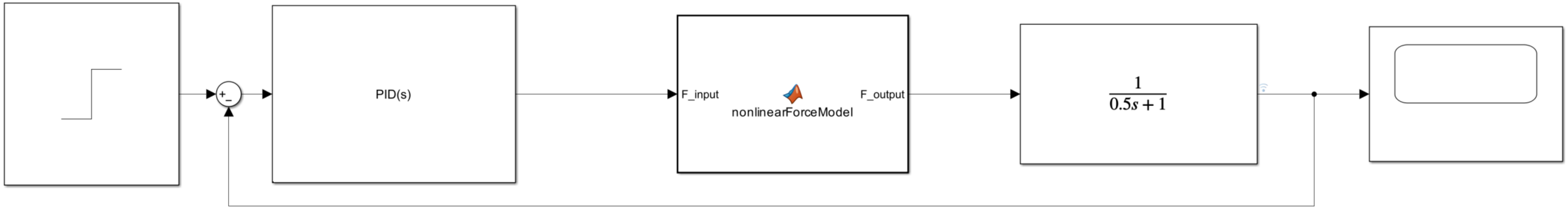

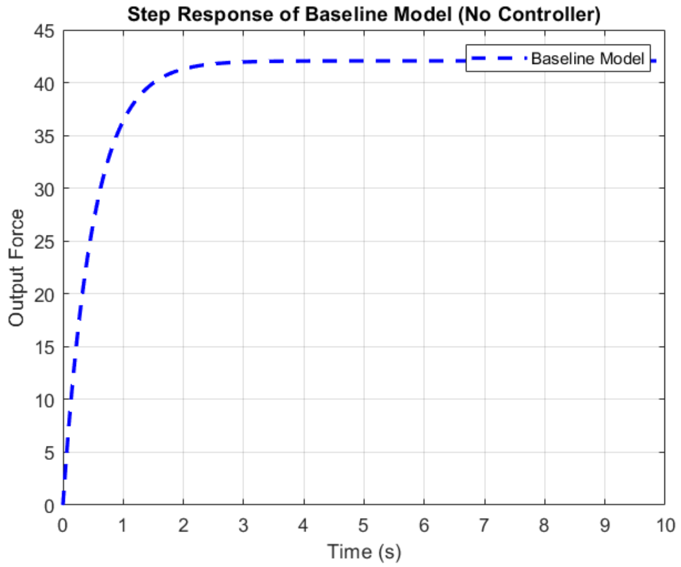

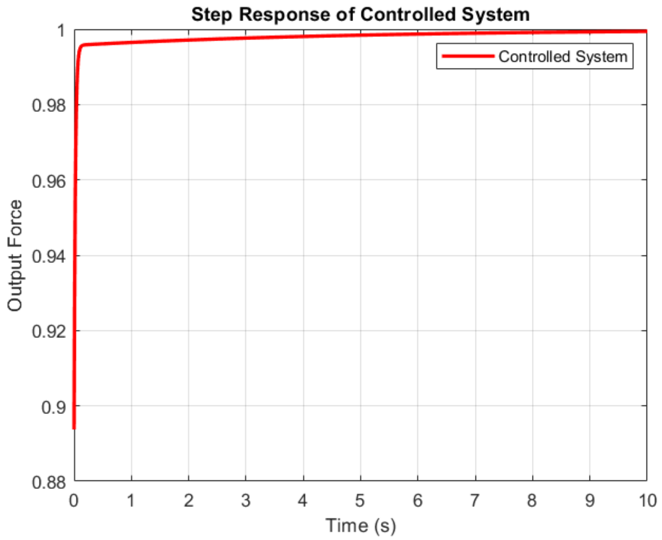

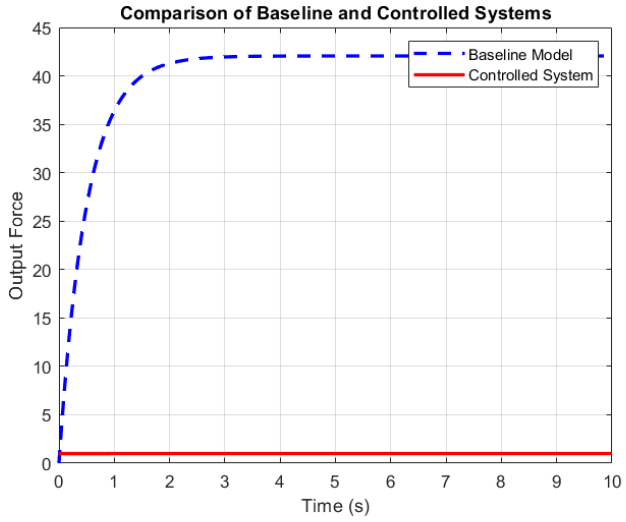

Finding the value of k (Torsional spring constant)

Spring Constant Calculation

Given the spring constant formula:

$$K = \frac{G \cdot J}{L}$$

where:

$G =$ Shear Modulus, $J =$ Moment of Inertia, $L =$ Length of Spring.

The Moment of Inertia J for a rectangular cross-section is given by:

$$J = \frac{b \cdot h^3}{12}$$

Substituting the values: - $b = 1.5\,\text{mm} = 1.5 \times 10^{-3}\,\text{m}$, - $h = 8\,\text{mm} = 8 \times 10^{-3}\,\text{m}$, - $L = 31\,\text{mm} = 31 \times 10^{-3}\,\text{m}$, - Young's Modulus $E = 3.5 \times 10^9\,\text{Pa}$, - Poisson's Ratio $\nu = 0.3$.

We calculate the Moment of Inertia J:

$$J = \frac{b \cdot h^3}{12} = \frac{1.5 \times 10^{-3} \cdot (8 \times 10^{-3})^3}{12} = 6.4 \times 10^{-12}\,\text{m}^4$$

Next, we calculate the Shear Modulus G using the relation:

$$G = \frac{E}{2(1+\nu)} = \frac{3.5 \times 10^9}{2(1+0.3)} = 1.35 \times 10^9\,\text{Pa}$$

Finally, the spring constant K is calculated as:

$$K = \frac{G \cdot J}{L} = \frac{1.35 \times 10^9 \cdot 6.4 \times 10^{-12}}{31 \times 10^{-3}} = 2.78\,\text{N/m}$$

Thus, the spring constant K is approximately:

$$K \approx 2.78\,\text{N/m}$$

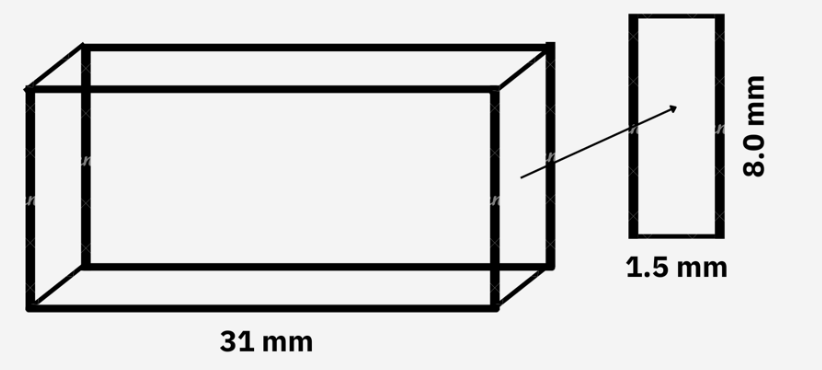

Refrences:
Timoshenko, S., & Goodier, J. N. (1970). Theory of Elasticity (3rd ed.). McGraw-Hill Education.
Khairurrijal, K. (2011). The dependence of the spring constant in the linear range on spring parameters. Physics Education, 46(5), 540–544.

Fatigue Analysis

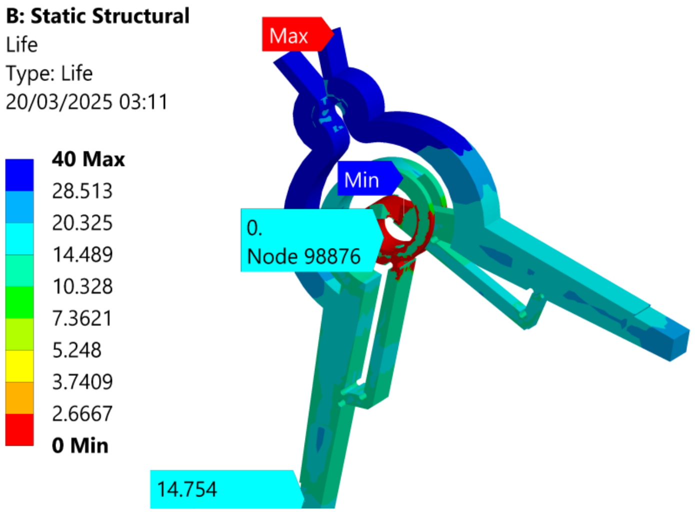

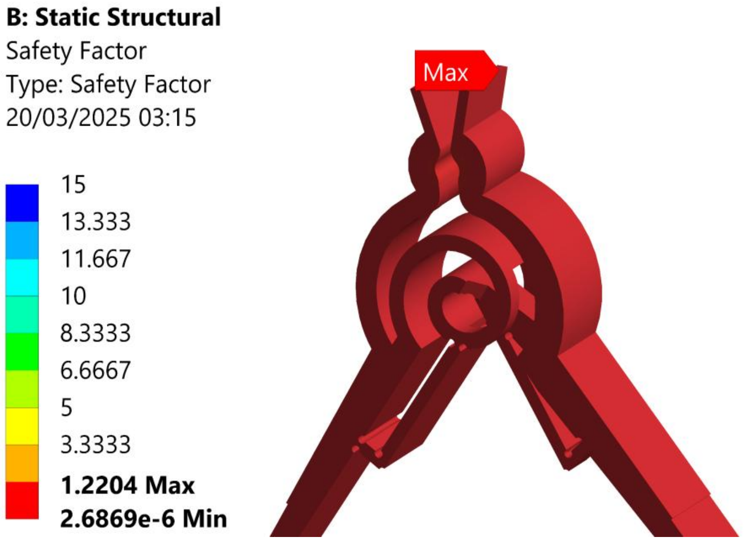

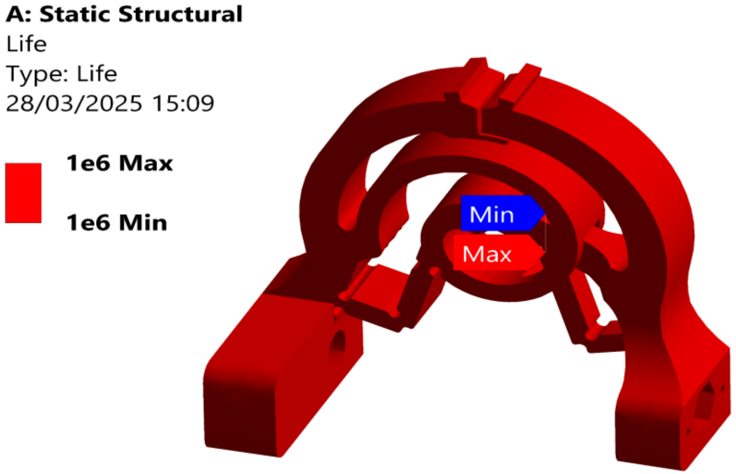

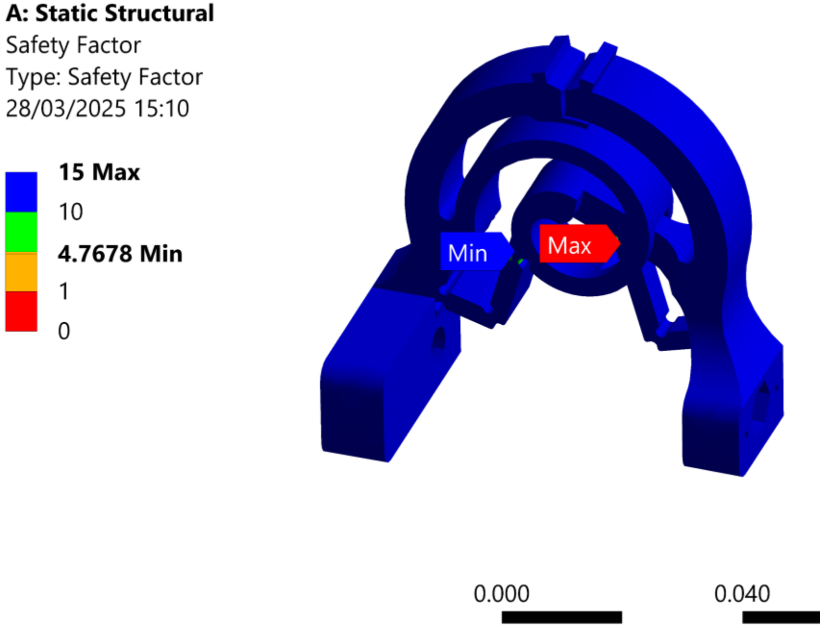

Mechanism comparisons

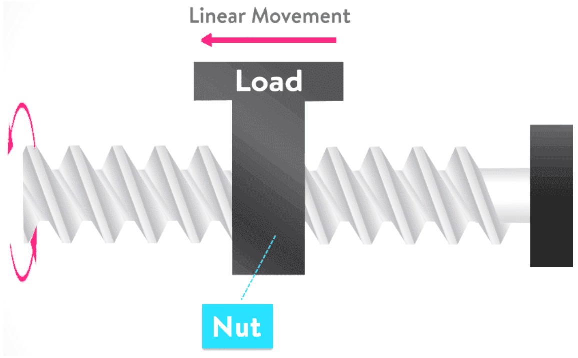

$$F_{\text{out}} = \frac{2\pi\,\eta\,T_{\text{in}}}{\text{pitch}}$$

$$Stroke - length = \frac{Pitch \times \theta}{360} = \frac{1 \times 180}{360} = 0.5mm$$

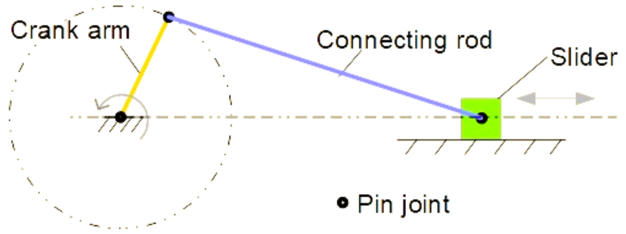

$$\boxed{F_{\text{out}} = \frac{T_{\text{in}}}{OA \cdot \cos(\theta)}}$$

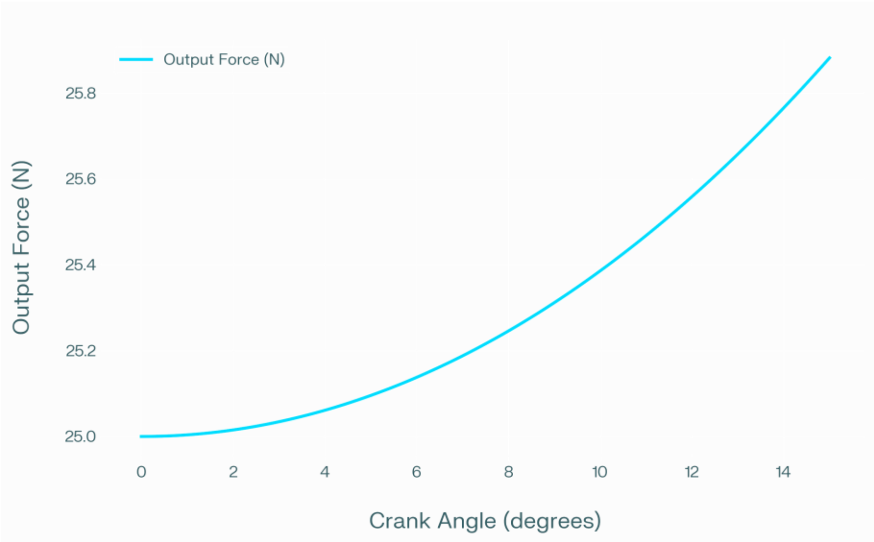

Mechanism	Input Torque (Nm)	Key Parameters	Max Output Force (N)
Slider-Crank	0.2	Crank radius = 8 mm (0.008 m)	25
Lead Screw	0.2	Pitch = 1 mm (0.001 m), Efficiency = 0.35	439.8

Design iterations

Worked

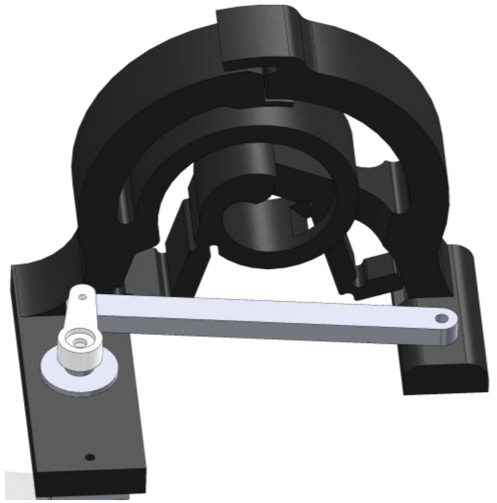

Failed

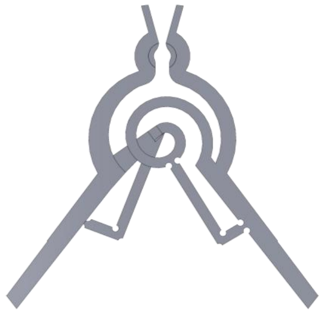

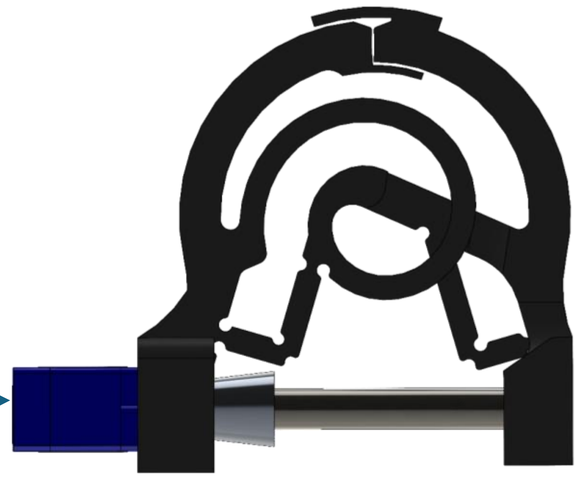

Modification:

- **Increased stroke length**
- **Less generated force**
- **Servo torque is limited to 0.456 Nm**

$$\boxed{F_{\text{out}} = \frac{T_{\text{in}}}{OA \cdot \cos(\theta)}}$$

Reason for Model Failure:

- Limited rotation of Servo
    - Stroke length
    - Hight force

$$Stroke-length = \frac{Pitch \times \theta}{360} = \frac{1 \times 180}{360} = 0.5mm$$

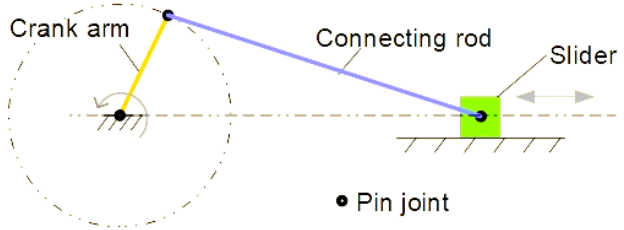

Control algorithm

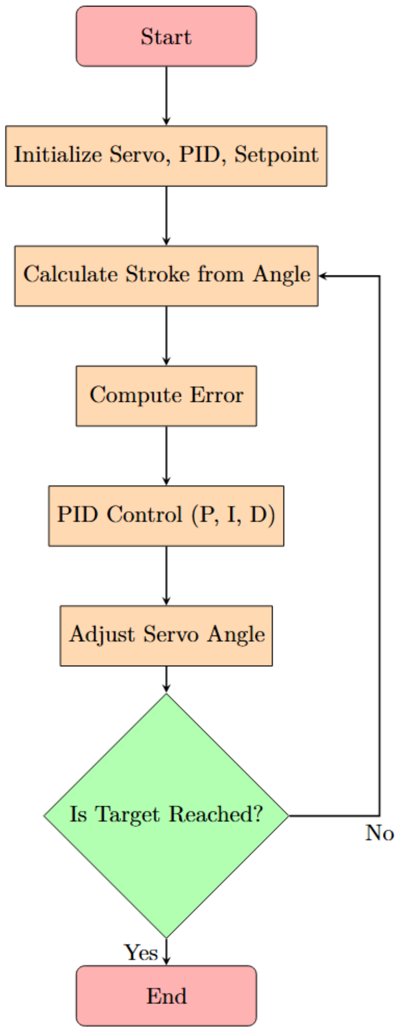

Algorithm 1 Crank-Slider Stroke Control with PID and Servo

Initialize Servo on pin 9
Define crank radius r and connecting rod length l
Set PID constants: K_p, K_i, K_d
Set initial target stroke position (`setpoint`)
Initialize stroke position (`currentX`), servo angle (`angle`)
Initialize PID state: `error`, `prevError`, `integral`, `derivative`
Initialize previous time variable
Flag `initialized` $\leftarrow$ `false`
procedure SETUP
  Start serial communication
  Attach servo to pin
  Set servo to $0°$
  Initialize `angle` and `prevTime`
procedure LOOP
  if not `initialized` **then**
    Move servo to $0°$
    Wait for 1 second
    `initialized` $\leftarrow$ `true`
    return
  Convert `angle` to radians θ
  `sinPart` $\leftarrow r \cdot \sin(\theta)$
  `insideSqrt` $\leftarrow l^2 -$ `sinPart`^{2}
  if `insideSqrt` < 0 **then**
    `insideSqrt` $\leftarrow 0$
  `currentX` $\leftarrow r \cdot \cos(\theta) + \sqrt{\texttt{insideSqrt}}$
  `error` $\leftarrow$ `setpoint` $-$ `currentX`
  $dt \leftarrow$ `currentTime` $-$ `prevTime`
  `integral` $\leftarrow$ `integral` $+$ `error` $\cdot\, dt$
  `derivative` $\leftarrow$ (`error` $-$ `prevError`)$/dt$
  `output` $\leftarrow K_p \cdot$ `error` $+ K_i \cdot$ `integral` $+ K_d \cdot$ `derivative`
  `angle` $\leftarrow$ `angle` $-$ `output`
  Clamp `angle` between $0°$ and $180°$
  Move servo to new `angle`
  Print debug info: target, current stroke, angle
  `prevError` $\leftarrow$ `error`
  `prevTime` $\leftarrow$ `currentTime`
  Wait 50 milliseconds

Hardware implementation

Lead screw based actuation

Experimental setup based on crank-slider actuation

Top view

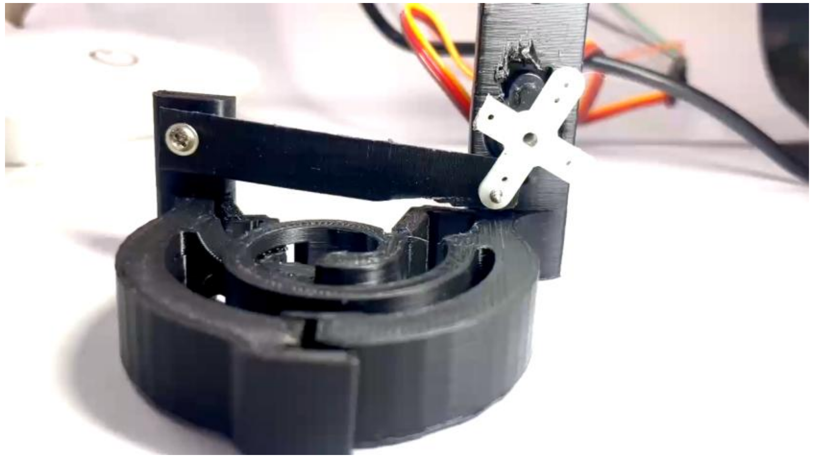

Front view

Experimental setup

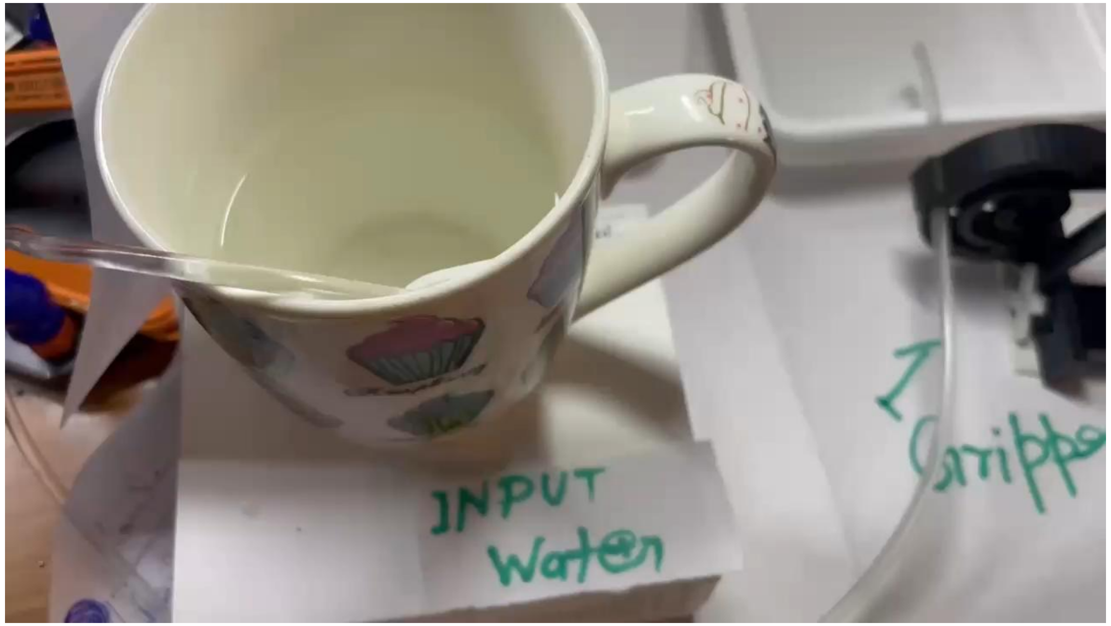

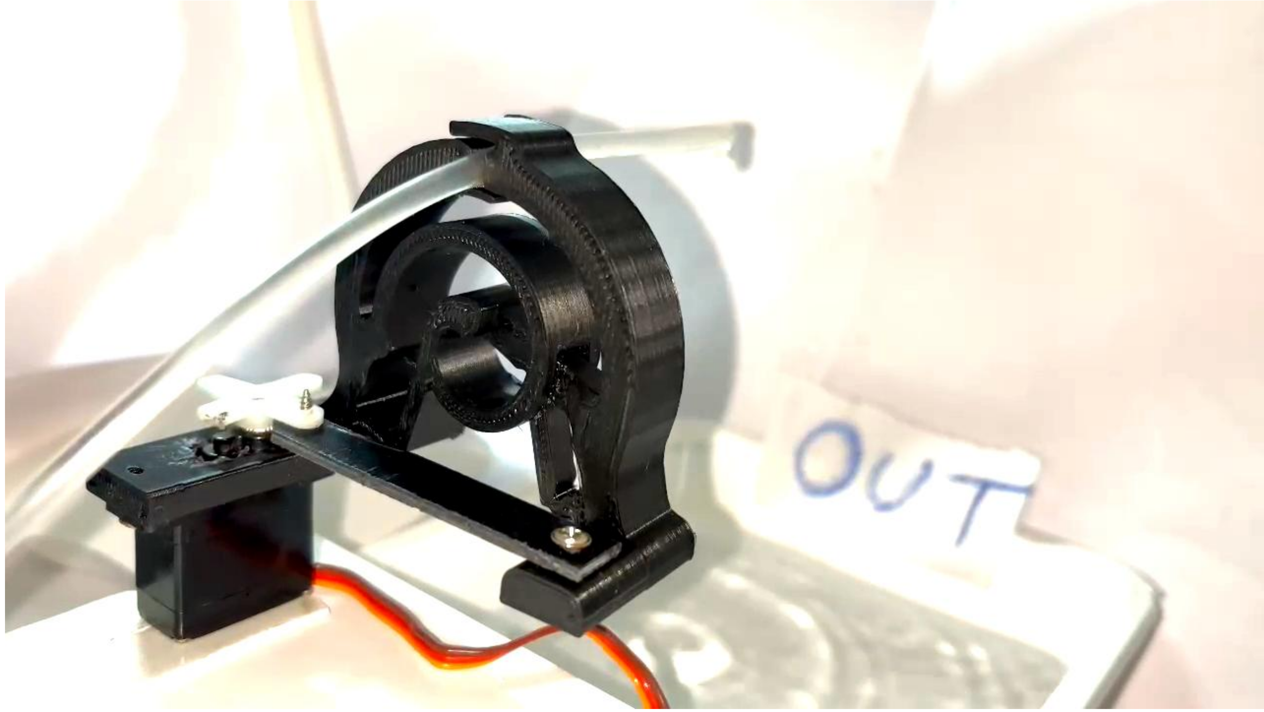

Results and conclusion

•The design incorporates a spiral spring as a compliant and energy-storing element, resulting in a higher lifecycle compared to other designs.

•Kinematic and force-deflection analyses confirm that the gripper provides a balanced relationship between input force and output displacement, essential for precise flow control in drug delivery systems.

•Finite Element Analysis (FEA) validates the structural robustness, with maximum deformation limited to 3.36 mm under operational loads, confirming the suitability of PLA+ for high-cycle fatigue applications1.

•Comparative mechanism analysis shows the lead screw actuation provides higher output force compared to slider-crank mechanisms under similar input torque, but with a trade-off in stroke length.

•Experimental hardware implementation and control algorithm (PID-based crank-slider stroke control) demonstrate the practical feasibility of the gripper for pipe flow control.

•No prior studies on this specific spiral spring-based compliant mechanism design were found in the literature, highlighting the novelty of this work.

•Future work should focus on optimizing the geometry and material at critical joints to improve fatigue life, and further experimental validation under real-world conditions

References

•Design and Implementation of a Compliant Gripper for Form Closure of Diverse Objects Kyler C. Bingham, Matthew Hessler, Safal Lama, and Taher Deemyad *Applied Sciences*, 2023, 13, 9677.
DOI: 10.3390/app13179677.

•Design and Analysis of a New Compliant Gripper for Microgripper Applications Mahmoud Magdy and Muhammed Gaafar *Proceedings of the 4th International Conference on Artificial Intelligence, Robotics and Control*, 2023.
DOI: 10.1109/AIRC57904.2023.10303209.

•Design of Compliant Gripper for Surgical Applications Libu George Babu and Bharanidaran Ramalingam *Australian Journal of Mechanical Engineering*, 2019. DOI: 10.1080/14484846.2019.1701396.

•A Bioinspired Soft Robotic Gripper for Adaptable and Effective Grasping Mariangela Manti, Taimoor Hassan, Giovanni Passetti, Nicolò D'Elia, Cecilia Laschi, and Matteo Cianchetti *Soft Robotics*, 2015, 2(3), 107-116. DOI: 10.1089/soro.2015.0009.

•A Compliant, Underactuated Hand for Robust Manipulation Lael U. Odhner, Leif P. Jentoft, Mark R. Claffee, Nicholas Corson, et al. *International Journal of Robotics Research*, 2014, 33(5), 736-752 DOI: 10.1177/0278364913514466.

•Design and Control of Monolithic Compliant Gripper Using Shape Memory Alloy Wires Ganapathy Then Mozhi, Kaliaperumal Dhanalakshmi, and Seung-Bok Choi *Sensors*, 2023, 23, 2052. DOI: 10.3390/s23042052.

•Nguyen, D.C., Phan, T.V. and Pham, H.T., 2018, November. Design and analysis of a compliant gripper integrated with constant-force and staOc balanced mechanism for micro manipulaOon. In 2018 4th InternaOonal Conference on Green Technology and Sustainable Development (GTSD) (pp. 291-295). IEEE. [11] hips://cults3d.com/en/3d-model/various/compliant-surgical-grippers [12] Xu, Q., 2013, December.

•Structure design of a new compliant gripper based on Scoi-Russell mechanism. In 2013 IEEE InternaOonal Conference on RoboOcs and BiomimeOcs (ROBIO) (pp. 1623-1628). IEEE. [13] hips://www.stlfinder.com/model/prbm-gripper-compliant-mechanism-I1eSHhvZ/4875343/ [14] Hao, G. and Zhu, J., 2019.

• Design of a monolithic double-slider based compliant gripper with large displacement and anO-buckling ability. Micromachines, 10(10), p.665.

References

- Trimmer, B.A.; Lin, H.-T.; Baryshyan, A.; Leisk, G.; Kaplan, D. Towards a Biomorphic Soft Robot: Design Constraints and Solutions. In Proceedings of the IEEE RAS and EMBS International Conference on Biomedical Robotics and Biomechatronics, Rome, Italy, 24–27 June 2012; pp. 599–605.
- 28. Pedersen, C.B.W.; Fleck, N.A.; Ananthasuresh, G.K. Design of a Compliant Mechanism to Modify an Actuator Characteristic to Deliver a Constant Output Force. J. Mech. Des. 2006, 128, 1101–1112. [CrossRef]

- Kumar, R.G.; Ananthasuresh, G.K. A Study of Mechanical Advantage in Compliant Mechanisms. In Proceedings of the 1st International and 16th National Conference on Machines and Mechanisms (iNaCoMM2013), Roorkee, India, 18–20 December 2013.

- Ruth, D.J.S.; Sohn, J.W.; Dhanalakshmi, K.; Choi, S.B. Control Aspects of Shape Memory Alloys in Robotics Applications: A Review over the Last Decade. Sensors 2022, 22, 4860.

- Ali, H.F.M.; Khan, A.M.; Baek, H.; Shin, B.; Kim, Y. Modeling and control of a finger-like mechanism using bending shape memory alloys. Microsyst. Technol. 2021, 27, 2481–2492.

- Ashrafiuon, H.; Jala, V.R. Sliding mode control of mechanical systems actuated by shape memory alloy. J. Dyn. Syst. Meas. Control. 2009, 131, 1–6.

- Timoshenko, S., & Goodier, J. N. (1970). Theory of Elasticity (3rd ed.). McGraw-Hill Education.

- Khairurrijal, K. (2011). The dependence of the spring constant in the linear range on spring parameters. Physics Education, 46(5), 540–544.